Weather and Climate Extremes 30 (2020) 100279

Contents lists available at ScienceDirect

Weather and Climate Extremes

journal homepage: http://www.elsevier.com/locate/wace

Drought-related hot summers: A joint probability analysis in the Iberian Peninsula

Andreia F.S. Ribeiro [a,*], Ana Russo [a], Célia M. Gouveia [a,b], Carlos A.L. Pires [a]

[a] Instituto Dom Luiz (IDL), Faculdade de Ciências, Universidade de Lisboa, Campo Grande, 1749-016, Lisboa, Portugal
[b] Instituto Português do Mar e da Atmosfera, Lisboa, Portugal

ARTICLE INFO

Keywords:
Droughts
Hot extremes
Compound events
Standardized precipitation evaporation index (SPEI)
Number of hot days (NHD)
Copulas
Conditional probability

ABSTRACT

Droughts and hot extremes are major sources of risk to several socio-economic activities and their impacts are expected to increase under future global warming. Moreover, the simultaneous or sequential occurrence (compound events) of different climate extremes may lead to the amplification of the associated impacts. Even though the latest efforts in assessing hot and dry extremes and their interactions, the development of models describing the joint behavior of climate extremes is still a challenge. To contribute to the understanding of these compound events, we propose to assess the probability of extremely hot summer days in the Iberian Peninsula (IP) being preceded by drought events in spring and early summer, based on their joint probability distribution through copula theory. The precursor drought hazard was characterized by the Standardized Precipitation Evaporation Index (SPEI) for the months of May, June and July for different timescales (3-, 6- and 9-months). The Number of Hot Days per month (NHD) summed over the months of July and August were considered for modelling. The dependence structure between SPEI and NHD was very well identified for the most of the IP's regions by asymmetrical copulas with upper tail dependence (except in northwestern regions), suggesting that compound hot and dry extremes are strongly associated. The results show that the transition from previous wet to dry regimes increases substantially the probability of exceeding summer NHD extreme values, depending on the region and the drought timescale and target month. The results suggest a spatial heterogeneity over the IP when characterizing the influence of water deficits on following summer extreme temperatures, whereas northeastern, western and central regions were found to be the regions more prone to summer hot extremes induced by dryness, in contrast to southwestern, northwestern and southeastern regions (depending on the month and the timescale). This study provides estimates of the probability of drought-related hot extremes in the summer of the IP for different regions, which could be an important tool for responsible authorities to mitigate the impacts magnified by the interactions between the different hazards.

1. Introduction

Drought and heat-related extremes (e.g. heatwaves, warm spells, hot days) are among the most influential climate hazards (Yuan et al., 2016; Zampieri et al., 2017; Lu et al., 2018) as they lead to a variety of impacts, such as exacerbation of fire risk and crop damage, causing several economic losses and adverse effects in human health and mortality (Gouveia et al., 2016; Mazdiyasni et al., 2017; Russo et al., 2017; Zampieri et al., 2017). The last IPCC reports on extreme events point out that unprecedented risk to humans and ecosystems are expected in a changing climate due to changes in precipitation and temperature regimes and extremes (IPCC, 2012, 2019), particularly if rapid and far-reaching transitions are not met in several economic sectors and areas (e.g. land, energy, industry, buildings, transport and cities) (IPCC, 2019).

Several studies have stressed the role played by the interplay between multiple climatic extremes, which may exacerbate the impacts of individual hazards (Zscheischler and Seneviratne, 2017; Zscheischler et al., 2018). For example, in the US although there is no significant trend in drought from 1960 to 2010, a substantial increase of concurrent droughts and heatwaves is observed during that period (Mazdiyasni and AghaKouchak, 2015). In Europe, the 2003 and 2010 extreme heatwaves were concurrent with serious drought conditions, causing more damage than extreme temperatures or extreme dryness would have caused

* Corresponding author.
E-mail address: afsribeiro@fc.ul.pt (A.F.S. Ribeiro).

https://doi.org/10.1016/j.wace.2020.100279
Received 14 January 2020; Received in revised form 4 August 2020; Accepted 24 August 2020
Available online 30 August 2020
2212-0947/© 2020 The Authors. Published by Elsevier B.V. This is an open access article under the CC BY-NC-ND license (http://creativecommons.org/licenses/by-nc-nd/4.0/).

individually (Hauser et al., 2015). In southern Greece, the extreme fire season of 2007 was driven by two complementary climatic extreme drivers: a major drought in preceding months and two major heatwaves in July and August (Gouveia et al., 2016). Also in the 2010 European summer, the previous conditions of low soil moisture in spring strongly amplified the magnitude of the devastating heatwave (Hauser et al., 2015). Similarly, in the case of the European heatwave in 2003, if soil moisture in previous spring levels had not been as close to climatology as they were, the temperatures could have been much higher (Whan et al., 2015). More recently, the catastrophic fire seasons of 2019 in Greece (NASA Earth Observatory, 2019a) and 2019/2020 in Australia are also pointed out to be associated with a drought exacerbation of hot conditions (NASA Earth Observatory, 2019b).

The processes involved in the soil moisture–temperature coupling and feedback have been addressed in a growing number of works (Miralles et al., 2014, 2019; Vogel et al., 2018; Mueller and Seneviratne, 2012; Seneviratne et al., 2010; Zampieri et al., 2009), with a clear relationship between dry/wet extremes and the frequency of hot extremes being identified in Southeastern Europe (Hirschi et al., 2011; Russo et al., 2019), in Iberian Peninsula (IP) (Mueller and Seneviratne, 2012; Russo et al., 2019), at almost all South America, Indonesia and Malaysia and extensive areas in North America (Mueller and Seneviratne, 2012). Consistent signal was identified, both with soil-moisture and soil-moisture proxies (Standardized Precipitation Evapotranspiration Index, SPEI, and Standardized Precipitation Index, SPI), with summer heat predictability being conditioned by preceding dry/wet anomalies (Russo et al., 2019), summer circulation anomalies (Quesada et al., 2012) and advected sensible heat which further strengthen local land–atmosphere feedbacks via soil desiccation (Schumacher et al., 2019). In this context, it is becoming vital to make use of a compound event approach for understanding the extreme impacts and investigate opportunities for predictability towards the mitigation of the consequences (Zscheischler et al., 2018).

This aim is even more important under the projected warming and drier last decades of the 21st century (IPCC, 2019), which may enhance the occurrence of more extreme compound events (Lu et al., 2018). In addition, the combined effects of the projected global warming have been particularly pronounced in specific regions, as is the case of the Mediterranean areas (Giorgi and Lionello, 2008). Among the Mediterranean areas, the IP is an outstanding example of how precursor soil-moisture deficits conditions are strongly related to the extreme hot temperatures in the following summer (Russo et al., 2019).

The present work goes a step further, by addressing a key property of compound extremes related to the existence of multivariate dependence structures between the involved variables (Hao et al., 2018b; Feng et al., 2019) through the use of a copula approach. The use of copulas is among the most recently applied techniques in multivariate dependence modelling in climate studies (Ribeiro et al., 2019a, 2019c; Zscheischler et al., 2017), and a couple of recent works have adopted copula-based methods to model the joint behavior of hot and dry extremes (Hao et al., 2017; Feng et al., 2019). Nevertheless, previous studies have characterized compound hot and dry extremes based on a panoply of approaches including event coincidence analysis (Donges et al., 2016; Rammig et al., 2015), multi-type point processes (in both space and time) (Toreti et al., 2019), the counting of number of simultaneous/consequential occurrences of multiple extremes (Hao et al., 2018b; Wu et al., 2019) and the use of an indicator approach such as the Standardized Dry and Hot Index (SDHI) (Hao et al., 2018a). In addition, artificial neural networks have been used to model non-linear proprieties and for prediction purposes (Ribeiro et al., 2019b; Russo et al., 2013).

The present preference for adopting a copula-based approach is manifold. The unique characteristics of copulas allow for a full characterization of the linear and nonlinear dependences between variables, aside from the shape of marginal distributions, allowing the characterization of the dependence structure between more than two variables (Durante and Sempi, 2015; Maity, 2018; Nelsen, 2006; Salvadori and De Michele, 2007). Moreover, besides the ability to characterize the overall dependence structure, copulas allow a flexible mensuration of the tail dependence, whose importance is critical when studying extreme events such as heatwaves and droughts (Serinaldi et al., 2009). In addition, the proprieties of copulas allow the estimation of conditional probabilities of one extreme event given the occurrence of another extreme event, constituting a valuable and attractive tool in risk analysis (Bokusheva et al., 2016; Ribeiro et al., 2019a).

The characterization of joint occurrence of extreme temperature and dryness is here performed based on the number of hot days (NHD) (Fischer et al., 2007; Zhang et al., 2011) and on the SPEI (Vicente-Serrano et al., 2010), respectively. The SPEI was used aiming to include the effect of evapotranspiration on drought monitoring, which is particularly relevant in the context of global warming (Beguería et al., 2014) and to take advantage of the index's multiscalar character. Moreover, in the IP the occurrence of dryer conditions is generally better characterized by SPEI rather than by simplest indices solely based on rainfall records, given the ability of including the impacts of warming processes (Vicente-Serrano et al., 2011; Peña-Gallardo et al., 2019). Nonetheless, the projected warmer climate is also likely to be enhancing the land-atmosphere feedbacks (Miralles et al., 2019; Seneviratne et al., 2010), and the precursor effects of low soil moisture availability also play a role on the following hot extremes. In this way and under the perspective of compound events, namely when feedback mechanisms are involved, the rationale of the present work is to highlight the adoption of statistical methods accounting for the joint behavior between the extreme variables, to contribute for the design of adaption measures. For this reason, the goal of the present work is to quantify the likelihood of occurrence of summer extremely hot days, preceded by the occurrence of droughts, preserving the dependence structure between NHD and SPEI in the IP for the period between 1950 and 2014. We intend to address the following key points: 1) if previous dryness is associated to extreme temperatures in the hottest months of the IP at the regional level 2) if it is possible to identify a spatial pattern of the dependence structures between spring and early summer SPEI and summer NHD and, 3) the probability of occurrence of extreme summer hot days over each region when preceded by drought conditions.

2. Materials and methods

2.1. Data and study area

The NHD was defined as the number of days with maximum temperature exceeding the 90th percentile. NHD was computed based on regularly gridded (0.5° resolution) values of daily maximum temperatures for 1950–2014 period from the ECAD-EOBS v14 daily dataset (Haylock et al., 2008). The computation of NHD, for the reference period of 1981–2010, followed the standard procedure determined by the Expert Team on Climate Change Detection and Indices (ETCCDI) (Karl et al., 1999; Peterson et al., 2001) and available through the R package from Zhang et al. (2011). This procedure can be summarized as follows: let TXij be the daily maximum temperature on day i in period j and let TXin90 be the calendar day 90th percentile centred on a 5-day window for the base period (Eq. 1). Then NHD is the count of days where:

$$TXij > TXin90 \quad (1)$$

The daily 90th percentile threshold TXin90 is robustly estimated from a sample of 150 days (5-day window × 30 years) for each day of interest to account for the mean annual cycle (Tank et al., 2009; Zhang et al., 2011). To avoid time discontinuities, the NHD were summed up at each grid point over the two hottest months in the IP, July and August.

The SPEI was calculated based on precipitation (P) and reference evapotranspiration (ET_0) from the CRU TS 4.01 database (0.5° resolution) for the 1950–2015 period (Harris et al., 2014) for 3 timescales (3-, 6-, 9-months). The principle of SPEI is to use the monthly difference D

between P and ET_0 to provide a measure of the water balance during a target month i:

$$D_i = P_i - ET_{0i} \quad (2)$$

This simple climatic water balance (Eq. 2) provides a more reliable measure of drought severity than only considering precipitation, as in other drought indicators (Beguería et al., 2014). Secondly, the calculated D_i is aggregated at the timescales k (months) using Eq. (3)

$$D_n^k = \sum_{i=0}^{k=1} P_{n-i} - ET_{0n-i}\ ,\ n \geq k \quad (3)$$

where n is the calculation frequency. To accumulate the previous months a Normal kernel function was applied to P and ET_0 to control the importance of the data before the target month, giving less weight to the past and to months near the target month (Beguería et al., 2014). The multiscalar propriety allows to contemplate the different response times of drought influence by reflecting the accumulated drought conditions of shorter or longer periods. For instance, a "SPEI-3 in May" is calculated in May based on the information of the two previous and current months, i.e., referring to March, April and May datum, therefore representing a 3-months timescale. Then, D was normalized using a log-logistic distribution to obtain SPEI which was used as proxy for surface moisture deficits to assess the impact of these deficits on the occurrence of subsequent hot days in the following summer months. Hence, the SPEI values for the months of May, June and July were considered to include the period preceding the hottest months and overlap the month of July to account for co-occurrent compound events. This procedure has been previously applied at a global scale by Mueller and Seneviratne (2012) using SPI and to the Mediterranean by Russo et al. (2019) using SPI and SPEI.

Due to the high spatial variability of drought conditions in the IP, here we determine main spatial-temporal drought modes based on SPEI over the IP applying a Principal Component Analysis (PCA) considering the months of May and June and the 3 timescales (3-, 6-, 9-months) (Figs. A.1, A.2 and A.3). For each timescale, the four principal components explaining most of the variance were rotated based on the varimax method (Hannachi et al., 2007 and references therein) and the main 3 were retained, leading to 9 different drought modes resulting from the 3 timescales. The 9 drought modes are considered for a k-means cluster analysis (Wilks, 2006) in order to capture different homogenous drought regions over the IP (Russo et al., 2015). The use of a k-means cluster analysis including all the timescales intends to summarize the drought behavior suitable to different response times of drought influence, allowing a further regional comparison among the different timescales. Based on the cluster analysis six different drought clusters are identified and spatial averages of SPEI and NHD were computed over each regional cluster.

To each pair of SPEI and NHD over each region the correlation is examined in terms of the Kendall's τ, which is a rank correlation test measuring the level of dependence between the datasets (i.e. independence test based on τ).

2.2. Joint probability analysis

Among multivariate analysis approaches, copula functions are quite popular (Mirabbasi et al., 2012; Lee et al., 2013; Li et al., 2015). The fundamentals of this methodology are provided by Sklar (1959), Nelsen (2006), Salvadori and De Michele (2007), Durante and Sempi (2015) and Maity (2018). The Sklar's theorem states that a joint probability distribution can be split into its univariate margins and a copula which

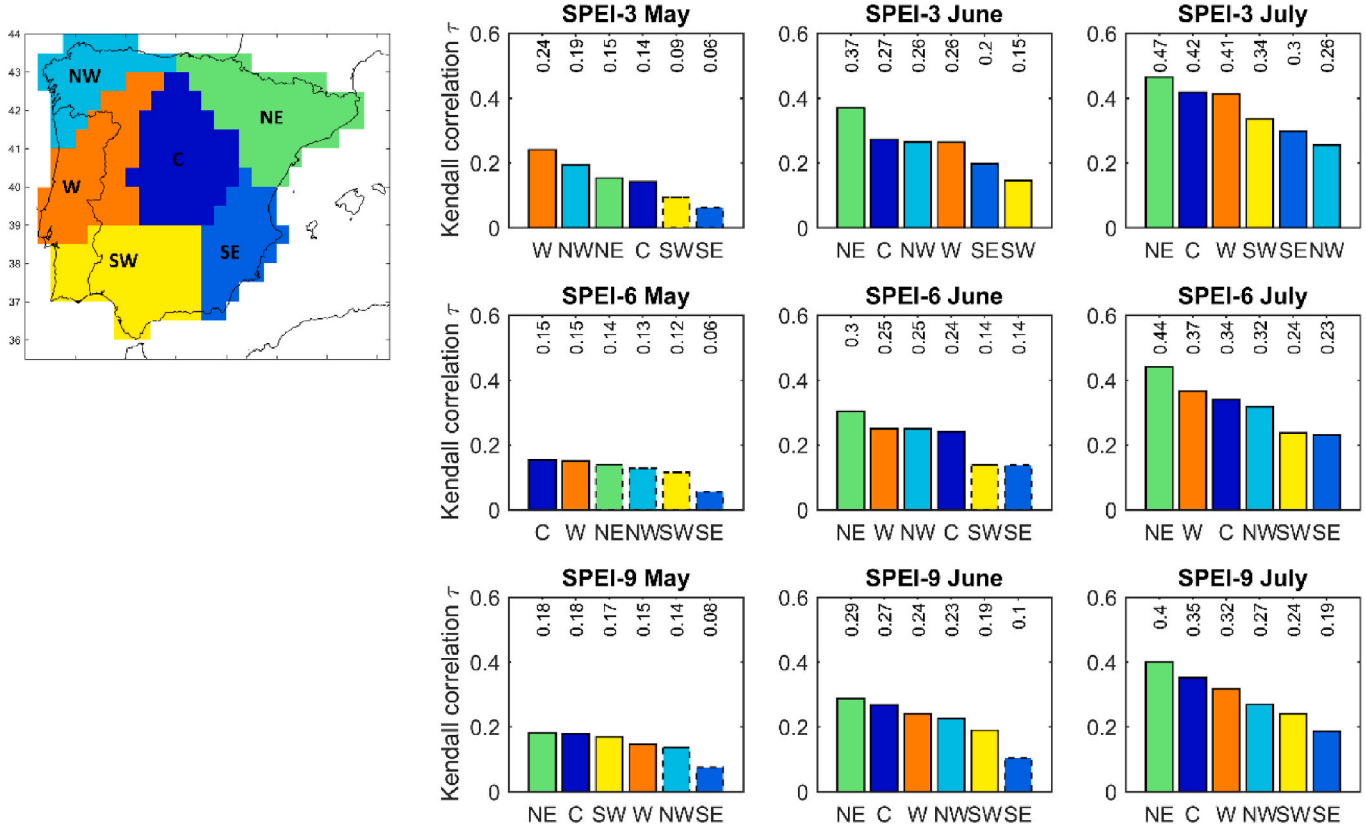

Fig. 1. Iberian Peninsula drought regions on the left map (northwestern (NW), northeastern (NE), central (C), western (W), southwestern (SW) and southeastern (SE) region) and respective Kendall's correlation coefficient (τ) between SPEI at 3-, 6- and 9-months' time scales in May, June and July and the sum of NHD in July and August for the 1950–2014 period over each regions. The bars are displayed in descending order of τ values and the dashed lines indicate the regions that failed the dependence test (p-value > 0.1) based on the Kendall's τ.

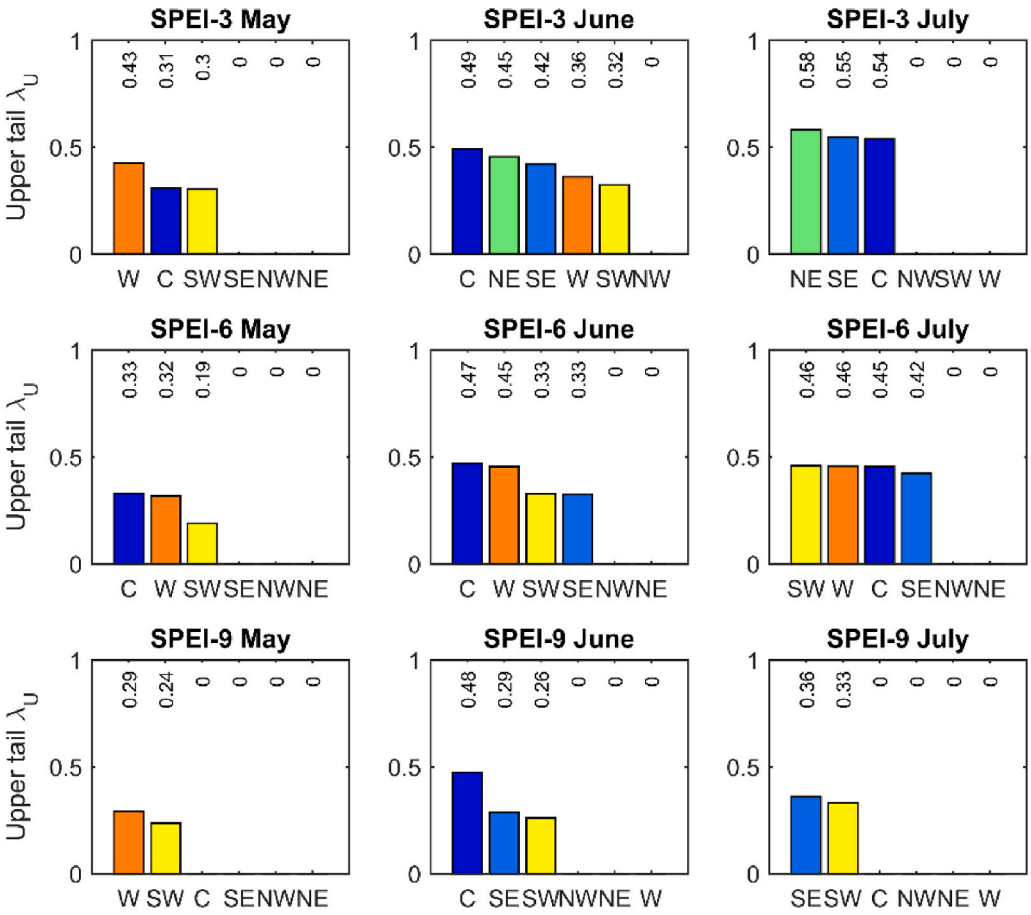

Fig. 2. Upper tail dependence parameter (λ_U) based on the selected copulas between SPEI at 3-, 6- and 9-months' time scales in May, June and July and the sum of NHD in July and August for the 1950–2014 period in the Iberian Peninsula at the regional level (northwestern (NW), northeastern (NE), central (C), western (W), southwestern (SW) and southeastern (SE) region). The cases characterized by copula models without upper tail dependence feature $\lambda_U = 0$ (Normal and Frank copulas, see Table A.1).

describes the dependence between the margins. Mathematically, given two correlated variables, X and Y, with marginal distributions $F_X(x)$ and $F_Y(y)$, uniform on the interval [0,1], a copula function C links these distributions to their joint probability distribution $F_{XY}(x, y)$ as follows:

$$F_{XY}(x, y) = C(F_X(x), F_Y(y)) \quad (4)$$

Here, X denotes the SPEI, Y the NHD and (x, y) are pairs of respective observations (Eq. 4). Copula functions show a great flexibility in modelling the dependence between variables with complex relationships and are adequate tools for modelling tailed events (extremes) in multivariate distributions (Mazdiyasni et al., 2017).

There is a range of copula families described in the literature allowing the modelling of several different shapes of radial asymmetry or symmetry, and different patterns of tail dependence. To each pair of SPEI and NHD we fit six different copulas: Normal, t, Clayton, Frank, Gumbel and Joe copulas. These well-documented copula functions belong to two distinct classes of copulas: Elliptical (Normal and t) and Archimedean (Clayton, Frank, Gumbel and Joe). The Archimedean copulas have an explicit formula with only one parameter and are quite popular given their ability in capturing a wider variety of joint dependence structures. The Clayton, Gumbel and Joe copulas describe an asymmetric tail behavior whereas Clayton copula can model lower tail dependence and Gumbel and Joe are able to model upper tail dependence. In contrast, the Normal, t and Frank copulas can capture symmetric dependencies, with the difference that the t copula allows dependence in the extremes in both lower and upper tails. Note that the Gumbel copula is both an Archimedean and Extreme-Value copula, and for this reason we consider also the Joe copula to capture upper tail dependencies. In addition, we aim to model the full distribution to capture all the events, and not only the extreme events.

When margins are continuous, then the corresponding copula is unique (Sklar, 1959). This work is a special case of bivariate copula modelling, related to the fact that one of the margins is noncontinuous (NHD), hence in such case the copula lacks uniqueness and biased estimates of the copula parameter may be obtained (Genest and Nešlehová, 2007; Trivedi and Zimmer, 2017). This is because the presence of ties in the samples can hide crucial features in the dependence structures and mislead the characterization of the full joint distribution. In order to fill this gap, we have used spatial averages of SPEI and NHD over each regional cluster to unleash the dominance of ties in the samples. In addition, the pseudo-observations (margins) were computed via the function pobs in R software, with the default tie's method "average", which replaces the ties by their mean. In this way, we argue that the use of the methodology described below is a good compromise between the complexity of characterization of the joint distribution in the discrete case and the limited sample size.

In this work, the copulas fits are performed based on a semi-parametric method, where the sample data is first transformed into uniform variables (u, v) using a nonparametric estimation (rank based) of the margins, and afterwards the copula parameters (θ) are estimated based on maximum likelihood. Due to the negative character of the correlation between SPEI and NHD (Russo et al., 2019), here we have considered margins of the symmetric (mirrored) SPEI data to simplify the copula modelling. Accordingly, drought conditions correspond to positive values of uniform SPEI and wet conditions correspond to negative values of uniform SPEI (the mirrored SPEI values). The copula model selection is performed based on the Bayesian information criterion (BIC) and the goodness of fit is performed by comparing with the respective empirical copula based on the Cramer-von Mises distance using a parametric bootstrap (Genest and Remillard, 2008). Table A.2 summarizes the p-values of the test with null hypothesis $H_0 : C_\theta \in C_n$ (C_θ is the selected parametric copula and C_n the respective empirical

copula) which are all greater than a significance level 0.1, suggesting the adequacy of the selected copulas.

Once the best fit for each SPEI and NHD combination is performed, uniformly distributed data is sampled from the selected copula models allowing for estimating the conditional probability of exceedance extreme summer NHD values when preceded by drought conditions and compared to when preceded by normal/wet conditions. Based on the estimated joint distributions, 10 000 samples of SPEI and NHD denoted u_{sim} and v_{sim}, respectively, are generated preserving the dependence structure between the variables. Note that the samples hold the mirrored values of SPEI, wherefore, drought conditions correspond the upper quantiles and wet conditions correspond to the lower quantiles. Hence, and since the simulations are uniform in the range [0,1], here drought is identified when u_{sim} is equal or above 0.8 (equivalent to the quantile 0.2 of SPEI (−0.84) according to the severity level associated with moderate drought by Agnew (2000)) and normal/wet conditions when u_{sim} is below 0.8. Afterwards, the correspondent NHD samples under drought conditions ($v_{sim,dry}$) and the NHD samples under normal/wet conditions ($v_{sim,wet}$) are considered. The conditional survival functions $1-F_{v_{sim,dry}}$ and $1-F_{v_{sim,wet}}$ are easily obtained by ordering the uniform samples ranging between [0,1] by descending order indicating the probabilities of exceedance (while the ascending order corresponds to the cumulative distribution functions $F_{v_{sim,dry}}$ or $F_{v_{sim,wet}}$ which indicates the probabilities of non-exceedance). To identify extreme summer NHD values the same quantile 0.8 used for SPEI is considered, and the correspondent probabilities of exceedance are estimated based on $1-F_{v_{sim,dry}}(0.8)$ and $1-F_{v_{sim,wet}}(0.8)$.

The associated uncertainties of the estimated probabilities of exceedance are addressed in terms of the uncertainty associated to the copula parameter and using the theoretical values inferred from the copula functions based on Eqs. 5 and 6 where $q = 0.8$ is the threshold used in both variables. In other words, the effect of the copula parameters inaccuracy is here considered in terms of the 95% confidence level and applying the formulas of conditional probabilities (Eqs. 5 and 6) using the lower and upper bound levels of the estimated copula parameters. With this procedure we aim to address the potential biased estimates of the copula parameter derived from the lack of unique copula in the case of a non-continuous margin.

$$\Pr(v \geq q \,|u \geq q) = \frac{1 - F_v(q) - F_u(q) + C(v=q, u=q)}{1 - F_u(q)} = \frac{1 - 2q + C(v=q, u=q)}{1-q} \tag{5}$$

$$\Pr(v \geq q \,|u < q) = \frac{F_u(q) - C(v=q, u=q)}{F_u(q)} = \frac{q - C(v=q, u=q)}{q} \tag{6}$$

The upper tail dependence λ_U for the chosen copulas will be evaluated and is obtained as the limit of Eq. 5 when q tends to 1 (Hartmann, 2004). For instance in the case of Gumbel and Joe copulas, the respective parametric estimators are given by $\lambda_U = 2 - 2^{\frac{1}{\theta}}$ (Nelsen, 2006).

3. Results

Six drought regions with different drought characteristics were identified applying a PCA and a cluster analysis over the IP (Fig. 1, left panel): northwestern (NW), northeastern (NE), central (C), western (W), southwestern (SW) and southeastern (SE) region. This regionalization is similarly to the ones obtained by Vicente-Serrano (2006) and Russo et al. (2015) and summarizes the IP's drought spatial heterogeneity including the 3-, 6- and 9-months SPEI timescales. In this way, the dependence between SPEI and NHD is here characterized over each drought region, in order to identify spatial patterns of drought influence on following summer (July and August) hot extremes.

Firstly, the relationship between SPEI at 3-, 6- and 9-months' time scales in May, June and July and the NHD in July and August over each region is examined in terms the Kendall's τ, and shown in Fig. 1. Note that the positive values are due to the use of mirrored SPEI values for simplicity, such that drought/wet conditions correspond to positive/negative values of SPEI. The dashed bar lines identify the regions that failed the dependence test (no rejection of null hypothesis $H_0: \tau = 0$), supporting that τ between SPEI and NHD is not significantly different from 0 at the significance level 0.1. Only the two southern regions (SW and SE) and the two northern regions (NW and NE) show no significant dependency between NHD and SPEI in rare cases when drought is characterized in May and June. In contrast, in July all the regions show significantly dependent values between NHD and SPEI, and the C and W regions show significant dependencies in all months and timescales.

Fig. 1 illustrates the regional dependence between spring and early summer SPEI and summer NHD, as obtained by Kendall's τ. In general, dependence increases with the co-occurrence in time between SPEI and NHD in all regions, since τ increases from May to July. In contrast, the differences between different SPEI timescales are not so evident, but the shorter timescale (3-months) are generally more dependent (but not in the same regions). The NE exhibits the strongest τ in almost all months and timescales (with the exception of SPEI-3 and -6 May), in contrast to the SE region that exhibits the lowest τ in almost all months and timescales (with the exception of SPEI-3 June and July, but still low). This pattern may be related with a strong vertical gradient in the eastern part of the IP and the importance of a regional analysis.

Afterwards we modeled the dependence structures between the drought indicator and following extreme temperatures by fitting archimedean and elliptical copula functions to estimate their joint probability. According to Fig. 2, a spatial pattern of the joint behavior between spring and early summer SPEI and summer NHD is characterized based on the type of selected copulas: most of the regions are dominated by asymmetrical dependence structures with upper tail dependence, while the NW is only characterized by symmetric dependence structures (Table A.1) and hence without upper tail dependence in all cases (Fig. 2). In fact, the use of bivariate copulas through its dependence structure can capture linear and nonlinear correlations among data. However, that dependence can be mostly concentrated in the main diagonal close the median, as in the case of Normal copulas, maximizing the linear correlation though having a vanishing tail dependence (as measured by λ_U). On the other hand, certain copulas enhance nonlinear

Table 1
95% confidence intervals (Eq. 5) of the conditional probabilities illustrated in Fig. 5.

		IB regions					
		C	SE	NW	NE	SW	W
	May	(0.2,0.51)	(0.14,0.37)	(0.25,0.47)	(0.21,0.44)	(0.2,0.51)	(0.29,0.58)
SPEI	June	(0.37,0.62)	(0.29,0.58)	(0.3,0.51)	(0.41,0.63)	(0.21,0.52)	(0.31,0.57)
3-month	July	(0.5,0.68)	(0.42,0.66)	(0.32,0.53)	(0.54,0.71)	(0.38,0.57)	(0.42,0.6)
	May	(0.21,0.52)	(0.14,0.37)	(0.18,0.41)	(0.21,0.44)	(0.2,0.46)	(0.2,0.52)
SPEI	June	(0.34,0.61)	(0.21,0.52)	(0.29,0.5)	(0.36,0.55)	(0.21,0.52)	(0.31,0.6)
6-month	July	(0.41,0.63)	(0.3,0.58)	(0.35,0.55)	(0.47,0.64)	(0.33,0.6)	(0.41,0.63)
	May	(0.25,0.47)	(0.15,0.38)	(0.19,0.39)	(0.23,0.46)	(0.2,0.49)	(0.2,0.5)
SPEI	June	(0.35,0.61)	(0.2,0.5)	(0.26,0.48)	(0.36,0.55)	(0.22,0.5)	(0.25,0.45)
9-month	July	(0.41,0.59)	(0.24,0.54)	(0.32,0.53)	(0.43,0.61)	(0.29,0.55)	(0.3,0.5)

Table 2
95% confidence intervals (Eq. 6) of the conditional probabilities illustrated in Fig. 6.

		IB regions					
		C	SE	NW	NE	SW	W
	May	(0.12,0.2)	(0.16,0.22)	(0.13,0.19)	(0.14,0.2)	(0.12,0.2)	(0.1,0.18)
SPEI	June	(0.09,0.16)	(0.11,0.18)	(0.12,0.18)	(0.09,0.15)	(0.12,0.2)	(0.11,0.17)
3-month	July	(0.08,0.13)	(0.09,0.14)	(0.12,0.17)	(0.07,0.12)	(0.11,0.15)	(0.1,0.15)
	May	(0.12,0.2)	(0.16,0.22)	(0.15,0.2)	(0.14,0.2)	(0.14,0.2)	(0.12,0.2)
SPEI	June	(0.1,0.16)	(0.12,0.2)	(0.12,0.18)	(0.11,0.16)	(0.12,0.2)	(0.1,0.17)
6-month	July	(0.09,0.15)	(0.11,0.18)	(0.11,0.16)	(0.09,0.13)	(0.1,0.17)	(0.09,0.15)
	May	(0.13,0.19)	(0.16,0.21)	(0.15,0.2)	(0.14,0.19)	(0.13,0.2)	(0.12,0.2)
SPEI	June	(0.1,0.16)	(0.13,0.2)	(0.13,0.19)	(0.11,0.16)	(0.12,0.2)	(0.14,0.19)
9-month	July	(0.1,0.15)	(0.12,0.19)	(0.12,0.17)	(0.1,0.14)	(0.11,0.18)	(0.12,0.17)

correlations with much more influence of the clustering of bivariate extremes as it is the case of Gumbel and Joe copulas (Table A.1). The choice of those copulas for certain pairs of (SPEI, NHD), shows thus the relevance of their nonlinear relationships. While previous similar works have analyzed the dependence between dry and hot conditions considering only Normal copulas (Hao et al., 2017, 2018b) or linear correlation analysis (Russo et al., 2019), we found that this combined phenomenon is very well identified for the most of the IP's regions by asymmetrical copulas with upper tail dependence (except in NW regions as shown in Table A.1 and Fig. 2).

In terms of timescales, the longest one (9-month) is mainly characterized by Normal or Frank copulas (Table A.1) and hence without upper tail dependence (Fig. 2) which can be explained by the information of the previous 9-months that can have less influence on the following summer hot extremes. In contrast, shorter timescales (3- and 6-months) are mainly described by Gumbel or Joe copulas (Table A.1), given that the drought conditions closest to the summer months may exert strongest influence in the following hot extremes. In fact, λ_U values are generally higher in June and July at both 3- and 6-months timescales (Fig. 2).

Some features in Fig. 2 and Table A.1 may contrast with Fig. 1. Even though the NE exhibits the strongest τ (Fig. 1) in most of the cases, in terms of λ_U is only more accentuated considering SPEI with the shorter timescale (Fig. 2). In fact, the relationship between summer NHD in the NE region and SPEI in June and July at 3-month timescale is described by a Gumbel model (extreme value copula), but the other months and timescales of SPEI in the NE feature Normal copulas (Table A.1). This means that in the NE a non-linear relationship between preceding drought and summer hot extremes dominates as we approach the cooccurrence of both extremes. This non-linear pattern in the NE between summer NHD and both SPEI-3 in June and July is characterized by an upper extreme dependence (Fig. 2) while the longest timescales are linear dependence structures although the large τ values in comparison to the other regions (Fig. 1). Since Kendall τ do not particularize

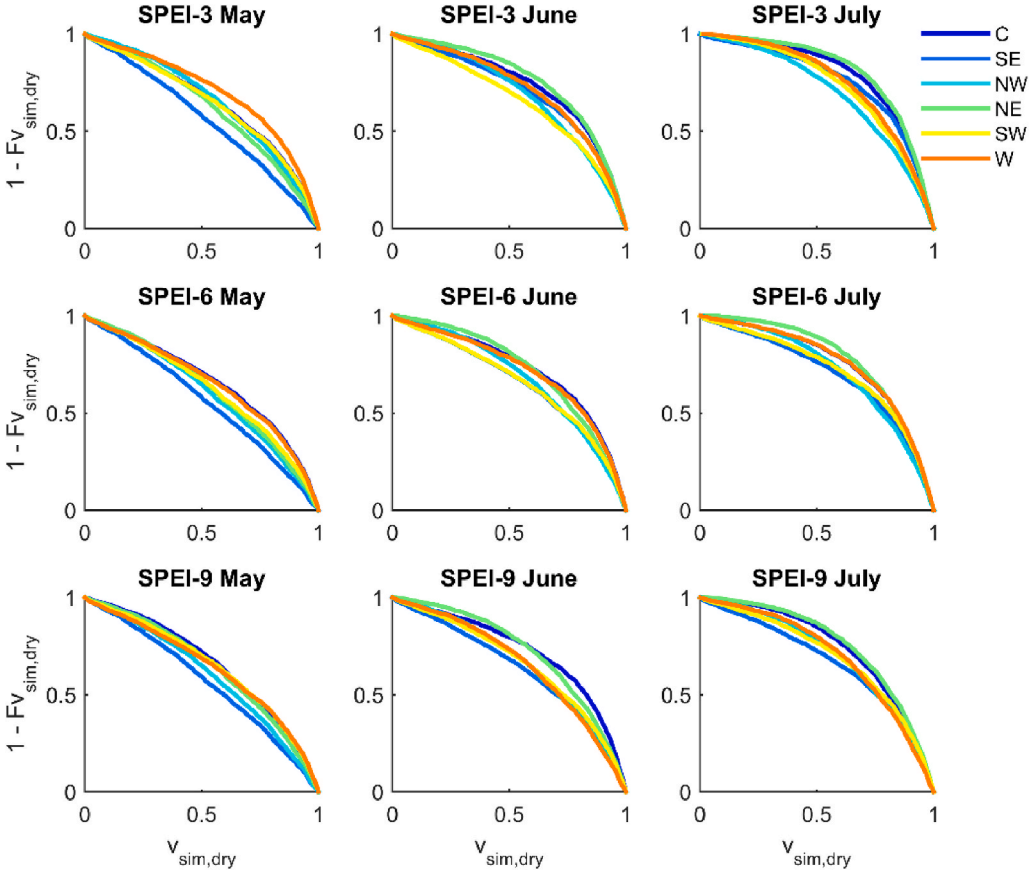

Fig. 3. Conditional survival curves based on the samples of summer NHD generated from the selected copulas (Table A.1) under dry conditions ($v_{sim,dry}$), indicating the exceedance probability $1 - F_{v_{sim,dry}}$ with SPEI at 3-, 6- and 9-months' time scales in May, June and July for each drought region in the Iberian Peninsula at the regional level (northwestern (NW), northeastern (NE), central (C), western (W), southwestern (SW) and southeastern (SE) region).

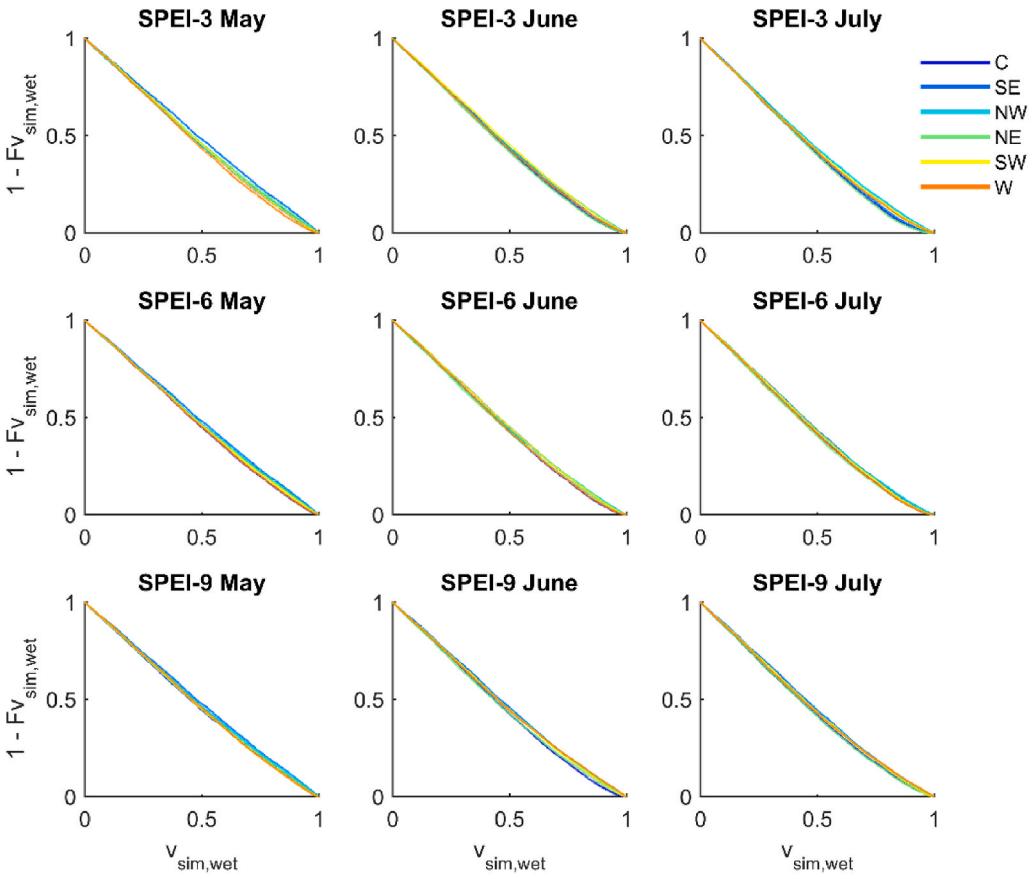

Fig. 4. Same as Fig. 3 for wet/normal conditions.

the tail dependence, it is perfectly possible to have non-vanishing τ and a small or even zero ??$_{??}$ In the case of the NE region at longer timescales of SPEI, the dependence is mostly near the median, which justifies the choice of a Normal copula (Table A.1), in contrast with the shorter timescale of SPEI during June and July dominated by a nonlinear relationship with upper tail dependence (Gumbel copula, Table A.1).

In addition, the pointed out vertical gradient in the eastern part (NE and SE) of the IP based on Kendall's τ (Fig. 1), is not so evident in terms of upper tail dependence at the 3-month timescale in June and July, which show similar λ_U values in NE and SE (Fig. 2). Nevertheless, the upper tail dependence in the SE in that case is slightly lower than in the NE, in agreement with lower τ values in the SE. This finding suggests that in comparison to the SE region, more extreme SPEI-3 in June and July drives more extreme summer NHD in the NE because is where occurs the strongest relationship in the upper right quadrant.

Another feature in Fig. 2 and Table A.1 contrasting Fig. 1, is in the SW region, which displayed rather modest Kendall's τ values but is the region with the higher number of Gumbel models describing the relationship between SPEI and NHD (Table A.1) and hence $\lambda_U \neq 0$ (Fig. 2). Thus, suggesting how variables with no apparent noteworthy correlation may show tail dependence in extreme values and hence how extreme hot summers are more likely to be induced by extreme drought than by normal drought in the SW. Still, in comparison to the other regions, a larger λ_U in the SW is only observed in one case, with July with a SPEI-6 (Fig. 2). Hence, a careful interpretation between correlation structure and extreme deviations is required because the higher number of cases characterized by an extreme value copula (Gumbel) in the SW could lead to the intuitive interpretation that is also where could occur the higher number of cases with strongest upper tail dependence.

The C region follows the SW in terms of the number of cases with non-linear dependency structures (Fig. 2) and when considering June drought conditions, the C region is where the highest λ_U values between SPEI and summer NHD occur at all timescales (Fig. 2). In the W region, the May drought conditions shows a modest τ values with NHD, but it's the region with highest λ_U at the 3- and 9-month timescales, being the region with highest predictive power of summer hot extremes.

In order to understand if summer hot extremes are exacerbated by the previous dryness, samples of SPEI and NHD generated from the selected copulas are further used to compare the summer NHD behavior when preceded by dry conditions ($v_{sim,dry}$) or by normal/wet conditions ($v_{sim,wet}$). Figs. 3 and 4 show the conditional survival functions of NHD under dry and normal/wet conditions, respectively. The probabilities of exceedance when preceded by dry conditions (Fig. 3) display a much larger spatial heterogeneity between regions in comparison to when preceded by normal/wet conditions (Fig. 4). Moreover, the survival curves in Fig. 3 are always more accentuated than survival curves in Fig. 4, suggesting that the probabilities of exceedance are always higher when NHD is preceded by dryness rather than by normal/wet conditions.

According to Fig. 3, the regions with more accentuated survival curves (higher NHD probabilities of exceedance) are the W, NE and C, depending on the month and timescale of SPEI. In the W region in particular, the NHD survival curves conditioned by drought conditions in May at all timescales are mainly on the top, which suggest that summer extreme temperatures in the W are mainly conditioned by spring drought. This is in agreement with the values of λ_U in Fig. 2, which point out a litoral influence of drought conditions in May as well. Similarly, in June the region with strongest λ_U is the C in all timescales, and the lead of C survival curves in June is also notable at 6- and 9-months. In contrast, the southern regions (SE and SW) and in some cases the NW region, are mainly associated to the lower survival curves, suggesting lower probabilities of exceedance (Fig. 3). Generally, the survivals curves are more accentuated from May to July (like Fig. 1), and

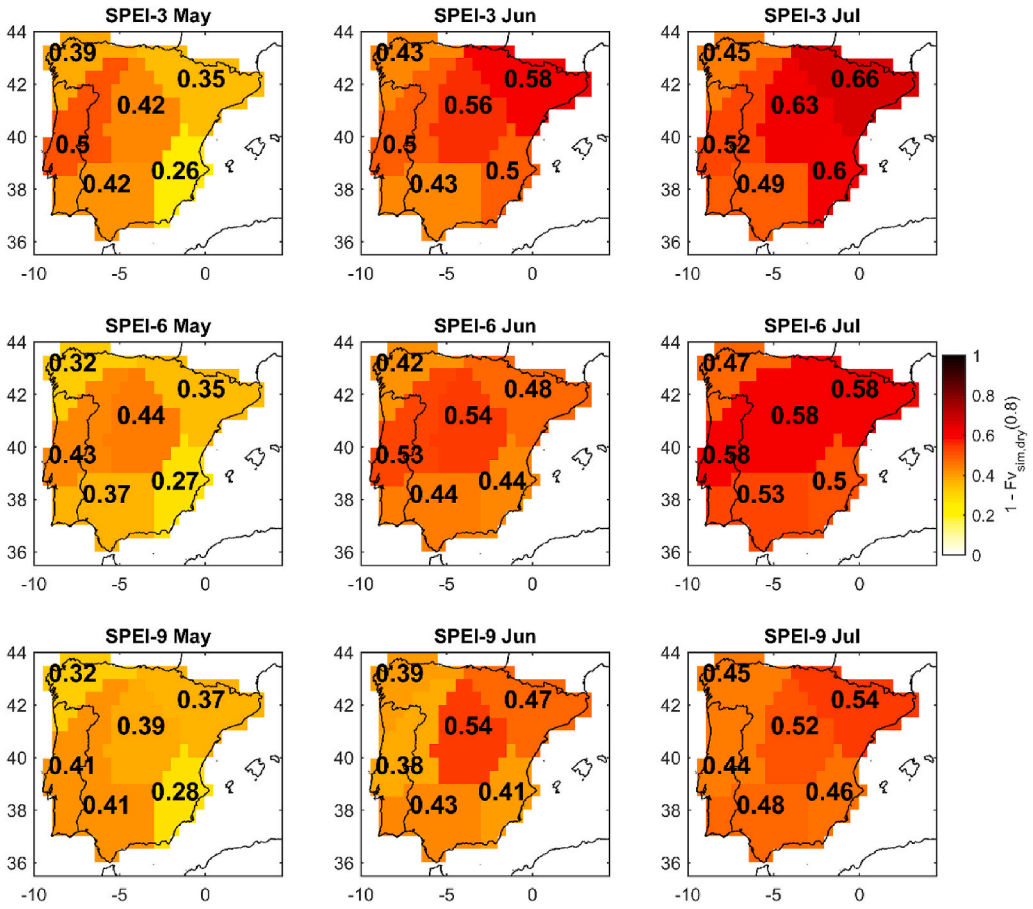

Fig. 5. Spatial patterns of the conditional probability of summer NHD exceeding the quantile $q = 0.8$ based on the copula simulations over each drought region when preceded by dryness ($1 - F_{v_{sim,dry}}(0.8)$) with SPEI at 3-, 6- and 9-months' time scales in May, June and July for each drought region in the Iberian Peninsula at the regional level. The associated 95% confidence intervals are shown in Table 1.

the differences between timescales is not so evident (Fig. 3). However, SPEI-3 in May and July may display larger differences between regions, while the curves in the other cases are closest between regions.

Based on the conditional survival functions (Figs. 3 and 4), the conditional probability of NHD exceeding the quantile $q = 0.8$ (the same threshold used here to define drought conditions) over each region when preceded by dry or normal/wet conditions is obtained by $1 - F_{v_{sim,dry}}(0.8)$ and $1 - F_{v_{sim,wet}}(0.8)$ and shown in Figs. 5 and 6, respectively. As expected from the previous shown survival curves (Figs. 3 and 4), the conditional probabilities are always higher when NHD is preceded by dryness (Fig. 5) rather than by normal/wet conditions (Fig. 6). Moreover, Fig. 5 displays a much larger spatial heterogeneity in comparison to Fig. 6, showing that the response of NHD extremes to dryness varies between regions over the IP territory (in contrast, the results suggest that the response of NHD extremes to wetness is similar between regions). This result suggests that water surplus do not influence as much as water stress influences summer extreme temperatures (in agreement with the fact that most of the regions feature models capturing the behavior in the upper extreme quantiles), and that the drought-related hot extremes varies significantly among regions in contrast to Fig. 6. In general, the probabilities of exceedance hot extremes at the $q = 0.8$ under dry conditions exceed 40% in most of the cases (except some regions in May and June 9-month), and under wet regimes the same chances are lesser than 19% in all cases.

According to Fig. 5, the regions with highest conditional probabilities of exceedance of hot extremes at the $q = 0.8$ when preceded by dryness are the W, NE and C regions (also in accordance with the survival functions in Fig. 3). When the SPEI values in July and previous months (depending the month time scale) point to dry condition, NE is the region with highest probability of occurring summer hot extremes at all timescales, while when June is a dry month, in the C region is slightly more likely of occurring summer hot extremes induced by dryness at 6- and 9-months timescales (Fig. 5). In dry Mays, the W region is where most of the following summer hot extremes may by induced by dryness as shown at all timescales (as previously shown in Fig. 2), despite being the second in raking in case of 6 months, but very close to the first in the ranking.

When the SPEI values in May point to dry condition, the SE region is the one with lowest probabilities of occurring hot extremes at all timescales (Fig. 5), while when the SPEI values in June and July point to dry conditions, NW is the region with lowest probabilities of occurring hot extremes in the following summer at the shorter timescales (3- and 6-months). At the longest timescale (9-months), the W region is the one with less likelihood of having hot extremes induced by drought conditions (in contrast with a dry May in the same region). Hence, the way how water stress affects the following summer hot extremes varies with the month, timescale of event and region (Fig. 5). The same conclusion is not so evident when the hottest months are preceded by water surplus or normal conditions (Fig. 6).

As conditional probabilities in Fig. 6 do not vary as much between months, timescales and regions as Fig. 5, maps illustrating the differences between dryness and wetness would have a similar coloring to Fig. 5. As so, the transition from previous wet to dry regimes has the biggest impact in July, followed by June and May. In the same way, the regions with largest changes in conditional probabilities from wet to dry regimes are NE, C and W regions, depending on the month and

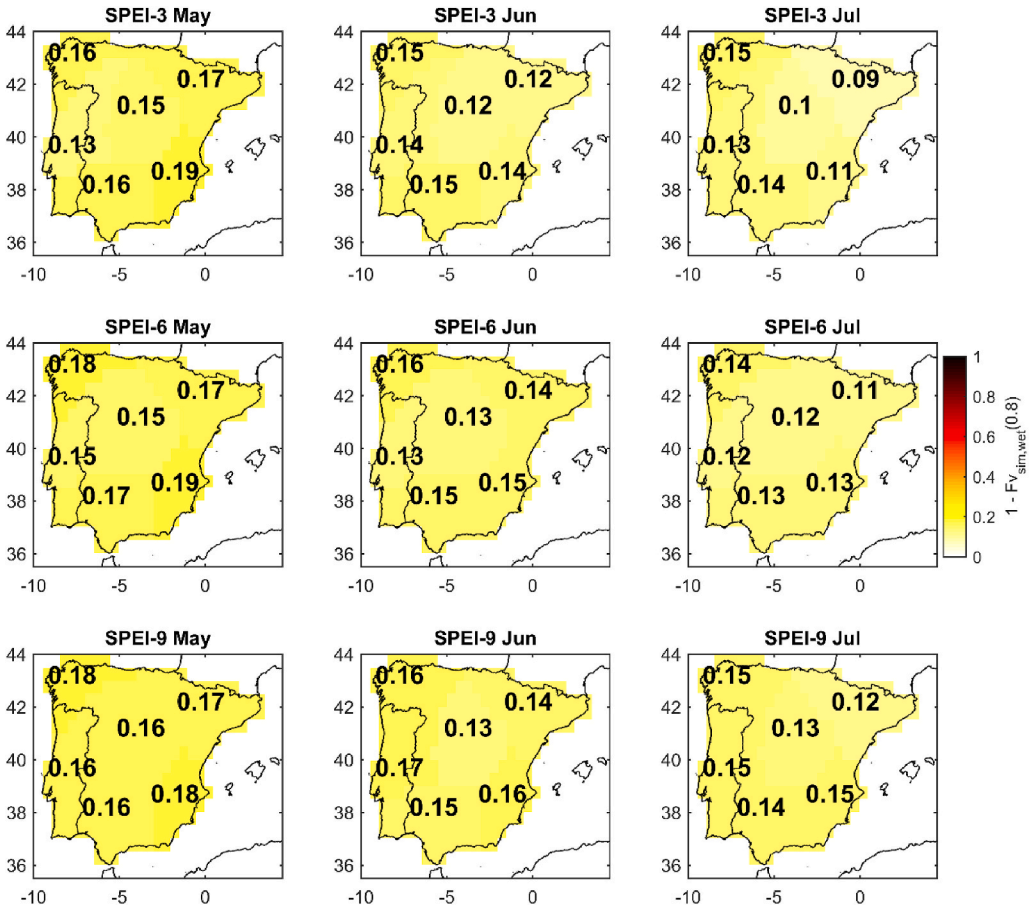

Fig. 6. Same as Fig. 5 for wet/normal conditions. The associated 95% confidence intervals are shown in Table 2.

timescale. In the case of the NE region in July at 3-month timescale the conditional probabilities of hot extremes may increase 57% when we transit from water surplus to deficits. In contrast, in the SE region in May at all timescales, the changes between Figs. 5 and 6 are only around 10%, because it is the region with highest likelihood of exceeding extreme values of NHD after soil moisture surplus in this case.

4. Discussion

According to the results, the influence of July dry conditions on summer hot extremes is more evident in NE regions, while May and June drought may influence more the number of warmer days in W and C regions, respectively. Moreover, the strength of this relation progresses from spring to summer and, subsequently, from W to C and NE (varying with timescale). Although the use of different methodologies makes difficult a direct comparison between studies, this conclusion agrees with previous works that found relationships between very dry conditions in spring and the evolution of warm days in W and C regions (Fernández-Montes et al., 2013). Additionally, the dominance of extreme temperatures in the NE part of the IP is also acknowledge in several studies (Fernández-Montes et al., 2013; El Kenawy et al., 2012; Rodríguez-Puebla et al., 2010), including during the 2003 heatwave (Díaz et al., 2006). The NE of the IP includes the Ebro valley, which is a semi-arid region with increasing drought severity (Ojeda et al., 2016; Vicente-Serrano et al., 2014; Vicente-Serrano and Cuadrat-Prats, 2007) and is experiencing an overall warming (El Kenawy et al., 2012). In contrast, in wet zones such as the NW where drought is not a major limiting factor (Ojeda et al., 2016) we do not identify a key influence on the occurrence of hot summers.

Other relevant mechanisms before and during heatwaves, such as the associated atmospheric circulation, was beyond the present study's scope, and it has been assessed by other authors which discuss the role played blocking patterns and ridge of high pressure (Sousa et al., 2018; Tomczyk et al., 2017). More recently, Sousa et al. (2019) have discussed the influence of Saharan air intrusions as a relevant mechanism for the occurrence of hot extremes in the IP. Other studies focus on the synoptic diagnosis of both heatwaves and droughts (Fink et al., 2006). Overall, the results suggest that when SPEI on previous months indicates dryness, rather than normal/wet conditions, the probabilities of occurring hot extremes during the following hottest months rises substantially. This result is in accordance with previous works, which identified in the IP significantly correlations between NHD and drought indicators, i.e., high values of NHD follows SPI/SPEI values associated to drought (Mueller and Seneviratne, 2012; Russo et al., 2019). Although these works pinpoint that there is a strong association and a certain predictability between preceding drought conditions and summer extreme temperatures, they lack a joint probability approach to address the risk of surpassing certain threshold conditions. The present approach has gone one step further by adopting a copula-based methodology which allowed for the estimation of conditional probabilities for specific thresholds of SPEI and NHD.

Although detrending is a usual procedure applied to distinguish between global warming and interannual variability, the application of a detrending procedure to the maximum temperature dataset used for the computation of NHD would be critical to define the summer hot extremes. A recent study by Turco et al. (2019) shows a comparison between detrending and not detrending maximum temperatures, with extreme cases such as the 2017 fire season in Portugal being missed when detrending is applied. One of the most important outcomes of this study is the proven ability to estimate the conditional probability of

drought-related hot extremes in the summer of the IP for different regions. Similarly, the study by Mueller and Seneviratne (2012) have determined the occurrence probability for above-average NHD for the globe, and found that after wet conditions is very unlikely to exceed above-average NHD in most of the areas of the world, including the IP.

5. Conclusions

The present study aimed to investigate the conditional probability of compound dry and hot extremes in the IP at the regional level, particularly summer hotness induced by previous dryness. The main findings of this study are summarized below:

- The dependence structure between SPEI and NHD is very well identified for the most of the IP's regions by asymmetrical copulas with upper tail dependence (except in NW regions), suggesting that compound hot and dry extremes are strongly associated.
- The transition from previous wet to dry regimes increases substantially the probability of exceeding NHD extreme values suggesting how summer hot extremes may be induced by previous soil moisture deficits.
- The relationships between summer NHD and previous SPEI increase from May to July, suggesting that the predictability power of a hot prone July and August increases as summer arrives.
- IP's drought spatial heterogeneity was found to be a main factor when characterizing the water stress influence on following summer extreme temperatures.
- In general, NE, W and C regions were found to be the regions with highest conditional probabilities of exceedance of hot extremes when preceded by dryness, in contrast to SW, NW and SE regions (depending on the SPEI month and timescale).

Future assessments of the amplified impacts of this kind of compound events in comparison with the impacts of individual drought or hotness is one of the targets for further work. Namely the impacts of compound drought and heat on the agricultural crops and how to prevent associated losses (Feng et al., 2019). Moreover, the combination of deficit precipitation and hot conditions may also exacerbate the fire risk and air pollution and understand the changes in these likelihoods are other promising lines for future research in the present climate chance context. Nonetheless, the development of such studies requires higher dimensional models with more complex structures and other methods rather than bivariate copulas.

Author's statement

AFSR, AR and CMG conceived the idea of the present study. AFSR analyzed the data, performed the statistical analysis, produced the figures and drafted the manuscript. AR and CMG supervised the work. CALP verified the analytical methods and designed the estimation of the conditional probabilities' uncertainty. AR performed the computations of SPEI and NHD. All the authors provided helpful insight in the discussion of the results and contributed to the design of the research and to the final paper.

Declaration of competing interest

The authors declare that they have no known competing interests or personal relationships that could have appeared to influence the work reported in this paper.

Acknowledgments

This work was done under the framework of the project IMPECAF (PTDC/CTA-CLI/28902/2017) funded by the Portuguese Foundation for Science and Technology (FCT). AFSR thanks FCT for the grant PD/BD/114481/2016.

Appendix

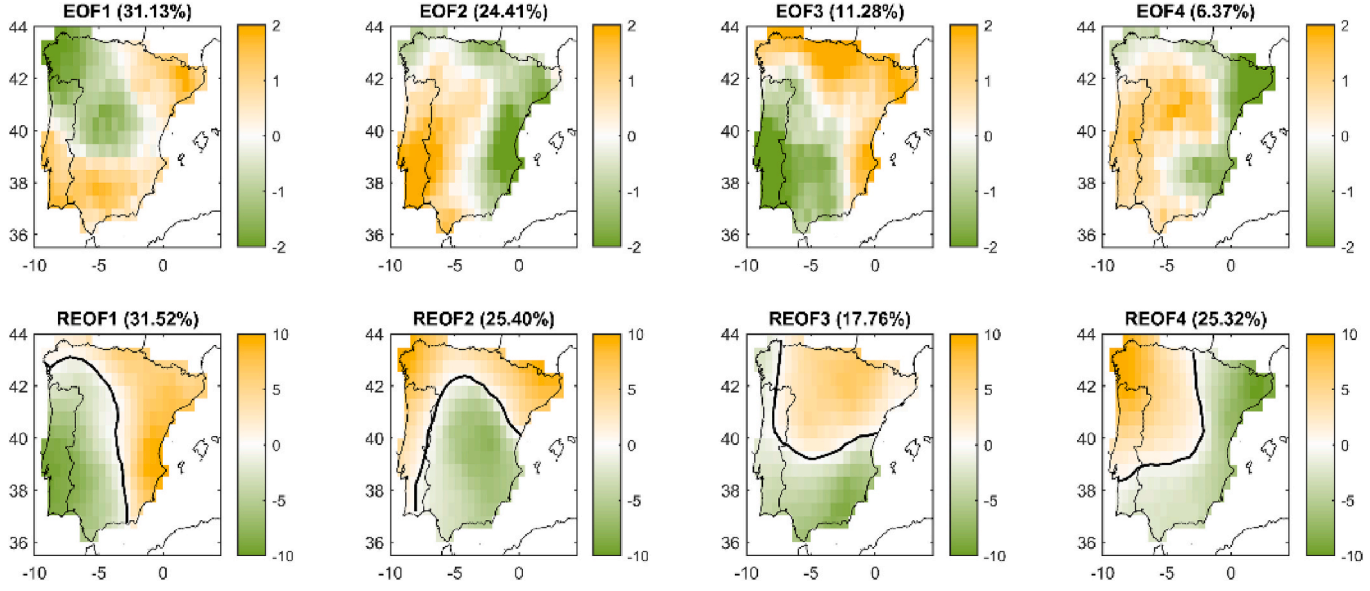

Figure A.1. Top: Four main Principal Component Analysis (PCA) modes considering the SPEI during May and June at the 3-month timescale. Bottom: Varimax rotated PCA modes, from which the main 3 were retained.

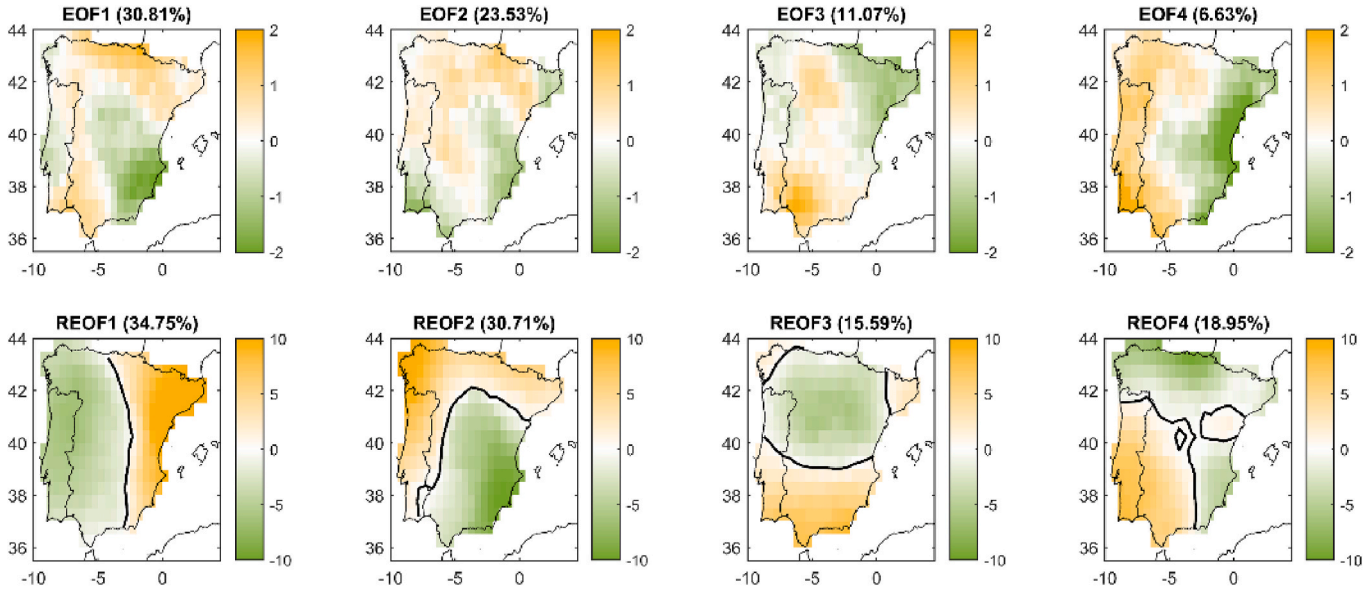

Figure A.2. Same as Fig. S1 for the 6-month timescale.

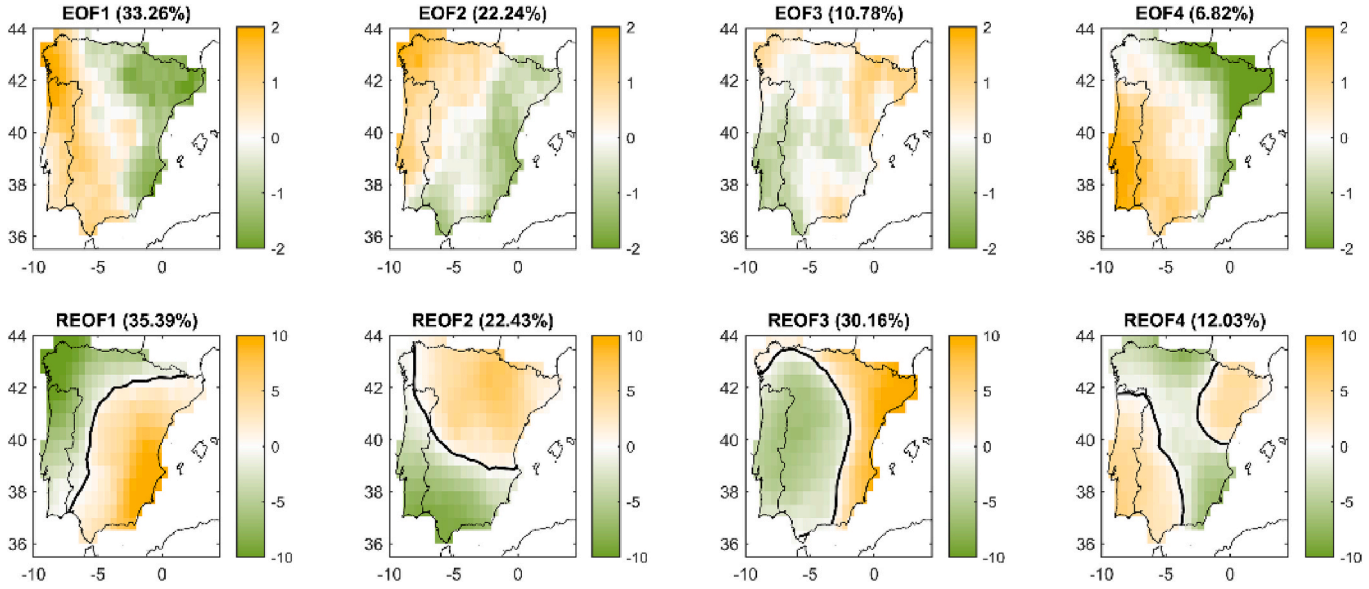

Figure A.3. Same as Fig. S1 for the 9-month timescale.

Table A.1
Copula models selected based on the Bayesian Information Criteria (BIC) to characterize the joint behavior between SPEI at 3-, 6- and 9-months' time scales in May, June and July and the sum of NHD in July and August for the 1950–2014 period in the Iberian Peninsula at the regional level (northwestern (NW), northeastern (NE), central (C), western (W), southwestern (SW) and southeastern (SE) region).

		IB regions					
		C	SE	NW	NE	SW	W
	May	Joe	Normal	Normal	Normal	Joe	Joe
SPEI	June	Joe	Joe	Normal	Gumbel	Joe	Gumbel
3-month	July	Gumbel	Joe	Normal	Gumbel	Normal	Normal
	May	Joe	Normal	Normal	Normal	Gumbel	Joe
SPEI	June	Joe	Joe	Normal	Normal	Joe	Joe
6-month	July	Gumbel	Joe	Normal	Normal	Joe	Gumbel
	May	Normal	Normal	Frank	Normal	Gumbel	Joe
SPEI	June	Joe	Joe	Normal	Normal	Gumbel	Frank
9-month	July	Normal	Joe	Normal	Normal	Gumbel	Frank

Table A.2
p-value of the copula models selected based on the Bayesian Information Criteria (BIC) to characterize the joint behavior between SPEI at 3-, 6- and 9-months' time scales in May, June and July and the sum of NHD in July and August for the 1950–2014 period in the Iberian Peninsula at the regional level (northwestern (NW), northeastern (NE), central (C), western (W), southwestern (SW) and southeastern (SE) region).

		IB regions					
		C	SE	NW	NE	SW	W
	May	0.30	0.21	0.38	0.38	0.87	0.55
SPEI	June	0.62	0.57	0.79	0.35	0.58	0.66
3-month	July	0.35	0.67	0.76	0.73	0.19	0.54
	May	0.30	0.62	0.17	0.55	0.63	0.54
SPEI	June	0.23	0.48	0.67	0.26	0.41	0.56
6-month	July	0.49	0.47	0.74	0.61	0.28	0.58
	May	0.14	0.35	0.19	0.45	0.51	0.42
SPEI	June	0.29	0.62	0.26	0.27	0.64	0.12
9-month	July	0.14	0.56	0.85	0.16	0.23	0.30

References

Agnew, C.T., 2000. Using the SPI to identify drought. Drought Netw. News 12, 6–12.

Beguería, S., Vicente-Serrano, S.M., Reig, F., Latorre, B., 2014. Standardized precipitation evapotranspiration index (SPEI) revisited: parameter fitting, evapotranspiration models, tools, datasets and drought monitoring. Int. J. Climatol. 34 (10), 3001–3023. https://doi.org/10.1002/joc.3887.

Bokusheva, R., Kogan, F., Vitkovskaya, I., Conradt, S., Batyrbayeva, M., 2016. Satellite-based vegetation health indices as a criteria for insuring against drought-related yield losses. Agric. For. Meteorol. 220, 200–206. https://doi.org/10.1016/j.agrformet.2015.12.066.

Díaz, J., García-Herrera, R., Trigo, R.M., Linares, C., Valente, M.A., De Miguel, J.M., Hernández, E., 2006. The impact of the summer 2003 heat wave in Iberia: how should we measure it? Int. J. Biometeorol. 50 (3), 159–166. https://doi.org/10.1007/s00484-005-0005-8.

Donges, J.F., Schleussner, C.F., Siegmund, J.F., Donner, R.V., 2016. Event coincidence analysis for quantifying statistical interrelationships between event time series: on the role of flood events as triggers of epidemic outbreaks. Eur. Phys. J. Spec. Top. 225 (3), 471–487. https://doi.org/10.1140/epjst/e2015-50233-y.

Durante, F., Sempi, C., 2015. Principles of Copula Theory. Taylor & F.

Feng, S., Hao, Z., Zhang, X., Hao, F., 2019. Probabilistic evaluation of the impact of compound dry-hot events on global maize yields. Sci. Total Environ. 689, 1228–1234. https://doi.org/10.1016/j.scitotenv.2019.06.373.

Fernández-Montes, S., Rodrigo, F.S., Seubert, S., Sousa, P.M., 2013. Spring and summer extreme temperatures in Iberia during last century in relation to circulation types. Atmos. Res. 127, 154–177. https://doi.org/10.1016/j.atmosres.2012.07.013.

Fink, A.H., Brücher, T., Krüger, A., Leckebusch, G.C., Pinto, J.G., Ulbrich, U., 2006. The 2003 European Summer Heatwaves and Drought – Synoptic Diagnosis and Impacts. Weather, pp. 209–216. https://doi.org/10.1256/wea.73.04.

Fischer, E.M., Seneviratne, S.I., Lüthi, D., Schär, C., 2007. Contribution of land-atmosphere coupling to recent European summer heat waves. Geophys. Res. Lett. 34 (6), 1–6. https://doi.org/10.1029/2006GL029068.

Genest, C., Nešlehová, J., 2007. A primer on copulas for count data. ASTIN Bull 37 (2), 475–515. https://doi.org/10.2143/ast.37.2.2024077.

Genest, C., Remillard, B., 2008. Validity of the parametric bootstrap for goodness-of-fit testing in semiparametric models. Ann. l'institut Henri Poincare Probab. Stat. 44 (6), 1096–1127. https://doi.org/10.1214/07-AIHP148.

Giorgi, F., Lionello, P., 2008. Climate change projections for the Mediterranean region. Global Planet. Change 63 (2), 90–104.

Gouveia, C.M., Bistinas, I., Liberato, M.L.R., Bastos, A., Koutsias, N., Trigo, R., 2016. The outstanding synergy between drought, heatwaves and fuel on the 2007 Southern Greece exceptional fire season. Agric. For. Meteorol. 218–219. https://doi.org/10.1016/j.agrformet.2015.11.023.

Hannachi, A., Jolliffe, I.T., Stephenson, D.B., 2007. Empirical orthogonal functions and related techniques in atmospheric science: a review. Int. J. Climatol. 27, 1119–1152. https://doi.org/10.1002/joc.1499Review.

Hao, Z., Hao, F., Singh, V.P., Ouyang, W., 2017. Quantitative risk assessment of the effects of drought on extreme temperature in eastern China. J. Geophys. Res. Atmos. 122 (17), 9050–9059. https://doi.org/10.1002/2017JD027030.

Hao, Z., Hao, F., Singh, V.P., Zhang, X., 2018a. Changes in the severity of compound drought and hot extremes over global land areas. Environ. Res. Lett. 13 (12) https://doi.org/10.1088/1748-9326/aaee96.

Hao, Z., Singh, V.P., Hao, F., 2018b. Compound extremes in hydroclimatology: a review. Water (Switzerland) 10 (6), 16–21. https://doi.org/10.3390/w10060718.

Harris, I., Jones, P.D., Osborn, T.J., Lister, D.H., 2014. Updated high-resolution grids of monthly climatic observations - the CRU TS3.10 Dataset. Int. J. Climatol. 34 (3), 623–642. https://doi.org/10.1002/joc.3711.

Hartmann, S.S., de V, C.G., 2004. Asset market linkages in crisis. Rev. Econ. Stat. 86 (1), 313–326 [online] Available from: https://www.jstor.org/stable/3211675.

Hauser, M., Orth, R., Seneviratne, S.I., 2015. Role of soil moisture vs . recent climate change for heat waves in western Russia. Geophys. Res. Lett. 43 (October), 2819–2826. https://doi.org/10.1002/2016GL068036.Received.

Haylock, M.R., Hofstra, N., Tank, A.M.G.K., Klok, E.J., Jones, P.D., New, M., 2008. A European daily high-resolution gridded data set of surface temperature and precipitation for 1950–2006, 113. https://doi.org/10.1029/2008JD10201.

Hirschi, M., Seneviratne, S.I., Alexandrov, V., Boberg, F., Boroneant, C., Christensen, O. B., Formayer, H., Orlowsky, B., Stepanek, P., 2011. Observational evidence for soil-moisture impact on hot extremes in southeastern Europe. Nat. Geosci. 4 (1), 17–21. https://doi.org/10.1038/ngeo1032.

IPCC, 2012. Managing the Risks of Extreme Events and Disasters to Advance Climate Change Adaptation.

IPCC, 2019. Special Report on Climate Change, Desertification, Land Degradation, Sustainable Land Management, Food Security, and Greenhouse Gas Fluxes in Terrestrial Ecosystems. SRCCL).

Karl, T.R., Nicholls, N., Ghazi, A., 1999. CLIVAR/GCOS/WMO workshop on indices and indicators for climate extremes - workshop summary. Climatic Change 42 (1), 3–7. https://doi.org/10.1023/A:1005491526870.

El Kenawy, A., López-Moreno, J.I., Vicente-Serrano, S.M., 2012. Trend and variability of surface air temperature in northeastern Spain (1920-2006): linkage to atmospheric circulation. Atmos. Res. 106, 159–180. https://doi.org/10.1016/j.atmosres.2011.12.006.

Lee, T., Modarres, R., Ouarda, T.B.M.J., 2013. Data-based analysis of bivariate copula tail dependence for drought duration and severity. Hydrol. Process. 27 (10), 1454–1463. https://doi.org/10.1002/hyp.9233.

Li, Y., Gu, W., Cui, W., Chang, Z., Xu, Y., 2015. Exploration of copula function use in crop meteorological drought risk analysis: a case study of winter wheat in Beijing, China. Nat. Hazards 77 (2), 1289–1303. https://doi.org/10.1007/s11069-015-1649-2.

Lu, Y., Hu, H., Li, C., Tian, F., 2018. Increasing compound events of extreme hot and dry days during growing seasons of wheat and maize in China. Sci. Rep. 8 (1), 1–8. https://doi.org/10.1038/s41598-018-34215-y.

Maity, R., 2018. Statistical Methods in Hydrology. Springer Trans. Civ. Environ. Eng. https://doi.org/10.1007/978-981-10-8779-0_10

Mazdiyasni, O., AghaKouchak, A., 2015. Substantial increase in concurrent droughts and heatwaves in the United States. Proc. Natl. Acad. Sci. 112 (37), 11484–11489. https://doi.org/10.1073/pnas.1422945112.

Mazdiyasni, O., AghaKouchak, A., Davis, S.J., Madadgar, S., Mehran, A., Ragno, E., Sadegh, M., Sengupta, A., Ghosh, S., Dhanya, C.T., Niknejad, M., 2017. Increasing probability of mortality during Indian heat waves. Sci. Adv. 3 (6), 1–6. https://doi.org/10.1126/sciadv.1700066.

Mirabbasi, R., Fakheri-Fard, A., Dinpashoh, Y., 2012. Bivariate drought frequency analysis using the copula method. Theor. Appl. Climatol. 108 (1–2), 191–206. https://doi.org/10.1007/s00704-011-0524-7.

Miralles, D.G., Teuling, A.J., Van Heerwaarden, C.C., De Arellano, J.V.G., 2014. Mega-heatwave temperatures due to combined soil desiccation and atmospheric heat accumulation. Nat. Geosci. 7 (5), 345–349. https://doi.org/10.1038/ngeo2141.

Miralles, D.G., Gentine, P., Seneviratne, S.I., Teuling, A.J., 2019. Land–atmospheric feedbacks during droughts and heatwaves: state of the science and current challenges. Ann. N. Y. Acad. Sci. 1436 (1), 19–35. https://doi.org/10.1111/nyas.13912.

Mueller, B., Seneviratne, S.I., 2012. Hot days induced by precipitation deficits at the global scale. Proc. Natl. Acad. Sci. U.S.A. 109 (31), 12398–12403. https://doi.org/10.1073/pnas.1204330109.

NASA Earth Observatory, 2019a. Drought exacerbates Australian fires. https://earthobservatory.nasa.gov/images/145599/drought-exacerbates-australian-fires.

NASA Earth Observatory, 2019b. Fires in Greece. https://earthobservatory.nasa.gov/images/39913/fires-in-greece.

Nelsen, R.B., 2006. An introduction to copulas. Springer Ser. Stat. 53 (9), 276. https://doi.org/10.1017/CBO9781107415324.004.

Ojeda, M.G.-V., Jiménez, E.R., Gámiz-Fortis, S.R., Castro-Díez, Y., Parra, M.J.E., 2016. Understanding the Drought Phenomenon in the Iberian Peninsula, vol. 13. Intech, i (tourism). https://doi.org/10.5772/57353.

Peña-Gallardo, M., Vicente-Serrano, S.M., Domínguez-Castro, F., Beguería, S., 2019. The impact of drought on the productivity of two rainfed crops in Spain. Nat. Hazards Earth Syst. Sci. 19, 1215–1234. https://doi.org/10.5194/nhess-19-1215-2019.

Peterson, T.C., Folland, C.C., Gruza, G., Hogg, W., Mokssit, A., Plummer, N., 2001. Report on the Activities of the Working Group on Climate Change Detection and Related Rapporteurs 1998–2001, Rep. WCDMP-47, WMO-TD 1071, (March), 143, doi:WMO, Rep. WCDMP-47,WMO-TD 1071.

Quesada, B., Vautard, R., Yiou, P., Hirschi, M., Seneviratne, S.I., 2012. Asymmetric European summer heat predictability from wet and dry southern winters and springs. Nat. Clim. Change 2 (10), 736–741. https://doi.org/10.1038/nclimate1536.

Rammig, A., Wiedermann, M., Donges, J.F., Babst, F., Von Bloh, W., Frank, D., Thonicke, K., Mahecha, M.D., 2015. Coincidences of climate extremes and anomalous vegetation responses: comparing tree ring patterns to simulated productivity. Biogeosciences 12 (2), 373–385. https://doi.org/10.5194/bg-12-373-2015.

Ribeiro, A.F.S., Russo, A., Gouveia, C.M., Páscoa, P., 2019a. Copula-based agricultural drought risk of rainfed cropping systems. Agric. Water Manag. 223. https://doi.org/10.1016/j.agwat.2019.105689.

Ribeiro, A.F.S., Russo, A., Gouveia, C.M., Páscoa, P., 2019b. Modelling drought-related yield losses in Iberia using remote sensing and multiscalar indices. Theor. Appl. Climatol. 136, 203–220. https://doi.org/10.1007/s00704-018-2478-5.

Ribeiro, A.F.S., Russo, A., Gouveia, C.M., Páscoa, P., Pires, C.A.L., 2019c. Probabilistic modelling of the dependence between rainfed crops and drought hazard. Nat. Hazards Earth Syst. Sci. 19 (12), 2795–2809. https://doi.org/10.5194/nhess-19-2795-2019.

Rodríguez-Puebla, C., Encinas, A.H., García-Casado, L.A., Nieto, S., 2010. Trends in warm days and cold nights over the Iberian Peninsula: relationships to large-scale variables. Climatic Change 100 (3), 667–684. https://doi.org/10.1007/s10584-009-9721-0.

Russo, A., Raischel, F., Lind, P.G., 2013. Air quality prediction using optimal neural networks with stochastic variables. Atmos. Environ. 79, 822–830. https://doi.org/10.1016/j.atmosenv.2013.07.072.

Russo, A., Gouveia, C.M., Páscoa, P., DaCamara, C.C., Sousa, P.M., Trigo, R.M., 2017. Assessing the role of drought events on wildfires in the Iberian Peninsula. Agric. For. Meteorol. 237–238. https://doi.org/10.1016/j.agrformet.2017.01.021.

Russo, A., Gouveia, C.M., Dutra, E., Soares, P.M.M., Trigo, R.M., 2019. The synergy between drought and extremely hot summers in the Mediterranean. Environ. Res. Lett. 14 (1), 014011 https://doi.org/10.1088/1748-9326/aaf09e.

Russo, A.C., Gouveia, C.M., Trigo, R.M., Liberato, M.L.R., DaCamara, C.C., 2015. The influence of circulation weather patterns at different spatial scales on drought variability in the Iberian Peninsula. Front. Environ. Sci. 3 (February), 1+. https://doi.org/10.3389/fenvs.2015.00001.

Salvadori, G. and De Michele, C.: On the use of copulas in hydrology: theory and practice, J. Hydrol. Eng, 12(4), 369–380, doi:10.1061/(ASCE)1084-0699.

Schumacher, D.L., Keune, J., van Heerwaarden, C.C., Vilà-Guerau de Arellano, J., Teuling, A.J., Miralles, D.G., 2019. Amplification of mega-heatwaves through heat torrents fuelled by upwind drought. Nat. Geosci. https://doi.org/10.1038/s41561-019-0431-6.

Seneviratne, S.I., Corti, T., Davin, E.L., Hirschi, M., Jaeger, E.B., Lehner, I., Orlowsky, B., Teuling, A.J., 2010. Investigating soil moisture-climate interactions in a changing climate: a review. Earth Sci. Rev. 99 (3–4), 125–161. https://doi.org/10.1016/j.earscirev.2010.02.004.

Serinaldi, F., Bonaccorso, B., Cancelliere, A., Grimaldi, S., 2009. Probabilistic characterization of drought properties through copulas. Phys. Chem. Earth 34 (10–12), 596–605. https://doi.org/10.1016/j.pce.2008.09.004.

Sklar, A., 1959. Fonctions de Répartition à n Dimensions et Leurs Marges. Inst. Stat. l'Université Paris 8, 229–231.

Sousa, P.M., Trigo, R.M., Barriopedro, D., Soares, P.M.M., Santos, J.A., 2018. European temperature responses to blocking and ridge regional patterns. Clim. Dynam. 50 (1–2), 457–477. https://doi.org/10.1007/s00382-017-3620-2.

Sousa, P.M., Barriopedro, D., Ramos, A.M., García-herrera, R., Espírito-santo, F., Trigo, R.M., 2019. Saharan air intrusions as a relevant mechanism for Iberian heatwaves: the record breaking events of August 2018 and June 2019, Weather Clim. Extrem (June), 100224. https://doi.org/10.1016/j.wace.2019.100224.

Tank, A.K., Zwiers, F.W., Zhang, X., 2009. Guidelines on Analysis of extremes in a changing climate in support of informed decisions for adaptation, WCDMP-No. 72, Clim. Data Monit., (WCDMP-No. 72) 52.

Tomczyk, A.M., Półrolniczak, M., Bednorz, E., 2017. Circulation conditions' effect on the occurrence of heatwaves in Western and Southwestern Europe. Atmosphere (Basel) 8 (2). https://doi.org/10.3390/atmos8020031.

Toreti, A., Cronie, O., Zampieri, M., 2019. Concurrent climate extremes in the key wheat producing regions of the world. Sci. Rep. 9 (1), 1–8. https://doi.org/10.1038/s41598-019-41932-5.

Trivedi, P., Zimmer, D., 2017. A note on identification of bivariate copulas for discrete count data. Econometrics 5 (1), 1–11. https://doi.org/10.3390/econometrics5010010.

Vicente-Serrano, S.M., 2006. Differences in spatial patterns of drought on different time scales: an analysis of the Iberian Peninsula. Water Resour. Manag. 20 (1), 37–60. https://doi.org/10.1007/s11269-006-2974-8.

Vicente-Serrano, S.M., Cuadrat-Prats, J.M., 2007. Trends in drought intensity and variability in the middle Ebro valley (NE of the Iberian peninsula) during the second half of the twentieth century. Theor. Appl. Climatol. 88 (3–4), 247–258. https://doi.org/10.1007/s00704-006-0236-6.

Vicente-Serrano, S.M., Begueria, S., Lopez-Moreno, J.I., 2010. A multiscalar drought index sensitive to global warming: the standardized precipitation evapotranspiration index. J. Clim. 23 (7), 1696–1718. https://doi.org/10.1175/2009JCLI2909.1.

Vicente-Serrano, S.M., López-Moreno, J.I., Drumond, A., Gimeno, L., Nieto, R., Morán-Tejeda, E., Lorenzo-Lacruz, J., Beguería, S., Zabalza, J., 2011. Effects of warming processes on droughts and water resources in the NW Iberian Peninsula (1930-2006). Clim. Res. 48 (2–3), 203–212. https://doi.org/10.3354/cr01002.

Vicente-Serrano, S.M., Lopez-Moreno, J.-I., Beguería, S., Lorenzo-Lacruz, J., Sanchez-Lorenzo, A., García-Ruiz, J.M., Azorin-Molina, C., Morán-Tejeda, E., Revuelto, J., Trigo, R., Coelho, F., Espejo, F., 2014. Evidence of increasing drought severity caused by temperature rise in southern Europe. Environ. Res. Lett. 9 (4), 044001 https://doi.org/10.1088/1748-9326/9/4/044001.

Vogel, M.M., Zscheischler, J., Seneviratne, S.I., 2018. Varying soil moisture-atmosphere feedbacks explain divergent temperature extremes and precipitation projections in central Europe. Earth Syst. Dyn. 9 (3), 1107–1125. https://doi.org/10.5194/esd-9-1107-2018.

Whan, K., Zscheischler, J., Orth, R., Shongwe, M., Rahimi, M., Asare, E.O., Seneviratne, S.I., 2015. Impact of soil moisture on extreme maximum temperatures in Europe. Weather Clim. Extrem. 9 https://doi.org/10.1016/j.wace.2015.05.001.

Wilks, D., 2006. In: Statistical Methods in the Atmospheric Sciences, second ed. Academic Press, Oxford, UK.

Wu, X., Hao, Z., Hao, F., Li, C., Zhang, X., 2019. Spatial and temporal variations of compound droughts and hot extremes in China. Atmosphere (Basel) 10 (2), 95. https://doi.org/10.3390/atmos10020095.

Yuan, W., Cai, W., Chen, Y., Liu, S., Dong, W., Zhang, H., Yu, G., Chen, Z., He, H., Guo, W., Liu, D., Liu, S., Xiang, W., Xie, Z., Zhao, Z., Zhou, G., 2016. Severe summer heatwave and drought strongly reduced carbon uptake in Southern China. Sci. Rep. 6 (January 2015), 1–12. https://doi.org/10.1038/srep18813.

Zampieri, M., D'Andrea, F., Vautard, R., Ciais, P., De Noblet-Ducoudré, N., Yiou, P., 2009. Hot European summers and the role of soil moisture in the propagation of mediterranean drought. J. Clim. 22 (18), 4747–4758. https://doi.org/10.1175/2009JCLI2568.1.

Zampieri, M., Ceglar, A., Dentener, F., Toreti, A., 2017. Wheat yield loss attributable to heat waves, drought and water excess at the global, national and subnational scales. Environ. Res. Lett. 12 (6), 064008 https://doi.org/10.1088/1748-9326/aa723b.

Zhang, X., Alexander, L., Hegerl, G.C., Jones, P., Tank, A.K., Peterson, T.C., Trewin, B., Zwiers, F.W., 2011. Indices for monitoring changes in extremes based on daily temperature and precipitation data. Wiley Interdiscip. Rev. Clim. Chang. 2 (6), 851–870. https://doi.org/10.1002/wcc.147.

Zscheischler, J., Seneviratne, S.I., 2017. Dependence of drivers affects risks associated with compound events. Sci. Adv. 3 (6), 1–11. https://doi.org/10.1126/sciadv.1700263.

Zscheischler, J., Orth, R., Seneviratne, S.I., 2017. Bivariate return periods of temperature and precipitation explain a large fraction of European crop yields. Biogeosciences 14 (13), 3309–3320. https://doi.org/10.5194/bg-14-3309-2017.

Zscheischler, J., Westra, S., Van Den Hurk, B.J.J.M., Seneviratne, S.I., Ward, P.J., Pitman, A., Aghakouchak, A., Bresch, D.N., Leonard, M., Wahl, T., Zhang, X., 2018. Future climate risk from compound events. Nat. Clim. Change 8 (6), 469–477. https://doi.org/10.1038/s41558-018-0156-3.